Implementation and Analysis of Quantum Fourier Transform in Image Processing

Article · March 2019

CITATIONS
0

READS
779

3 authors:

Ola Al-Ta'ani
Yarmouk University
4 PUBLICATIONS **17** CITATIONS
SEE PROFILE

Ali Mohammad Alqudah
Yarmouk University
25 PUBLICATIONS **38** CITATIONS
SEE PROFILE

Manal Al-bzoor
Yarmouk University
14 PUBLICATIONS **150** CITATIONS
SEE PROFILE

JJEE
Volume 5, Number 1, 2019
Pages 11-26
Jordan Journal of Electrical Engineering
ISSN (Print): 2409-9600, ISSN (Online): 2409-9619

Implementation and Analysis of Quantum Fourier Transform in Image Processing

Ola Al-Ta'ani[1a], Ali Mohammad Alqudah[2], Manal Al-Bzoor[1]

[1]Department of Computer Engineering, Yarmouk University, Irbid, Jordan
[2]Department of Biomedical Systems and Informatics Engineering, Yarmouk University, Irbid, Jordan
[a]e-mail: olataani@yu.edu.jo

Received: October 18, 2018 *Accepted: December 2, 2018*

Abstract— There is a growing interest in quantum image processing (QImP) that rose from the desire to exploit the properties of quantum computing to improve the performance of classical techniques and their applications. While Fourier transform (FT) is one of the most important algorithms used in signal and image processing, it is also considered a key ingredient in most modern quantum algorithms. A quantum Fourier transform (QFT) differs from the classical (FT) in that it takes a quantum state in which the initial data have been encoded into probability amplitudes. It alters the amplitudes of the corresponding discrete Fourier transform (DFT). The classical algorithms take an entire complex valued vector; and return the entire DFT in the form of another vector of the same length. These computations are proven to be exponentially faster on quantum computers than those of classical computers. In this paper, we demonstrate a framework of QImP where image information including pixel values and their positions are encoded in a pure quantum state. This framework is more efficient in terms of the number of the required qubits. This framework is supported with an experimental demonstration of the quantum image encoding, processing, and decoding along with a detailed comparison with the conventional ones. Quality assessment of the restored images is also provided where different common measures such as Mean-Squared Error (MSE), Peak Signal-to-Noise Ratio (PSNR), and Structural Similarity Index (SSIM) are used. In general, our experimental results, which were conducted on a classical computer, show similarity of quantum image transformation to its classical counterpart.

Keywords— Quantum computation, quantum image processing, quantum Fourier transform, quantum image representation.

I. INTRODUCTION

Image processing is one of the largest research paradigms in computer science and engineering. It is most attractive to researchers who are keenly interested in applications that directly affect human life such as in medical imaging [1], [2]. Research in this field has recently flourished due to the high availability of images datasets for human interpretation, high ability of techniques improvement, and the use of processed scene data for artificial intelligence processes. However, most of the current image processing techniques are considered time consuming for a real time application that is sensitive to the incorporated delays.

In the last decade, QImP has witnessed a rise as an emerging field in quantum computing that provided innovative solutions to some challenges faced by current image processing techniques. In general, QIP has three steps as shown in Fig. 1. First, store the image into a quantum system, which is also known as quantum image preparation. This step is the classical-quantum interface. Then, process the quantum image which is the main step of QIP. It means using a quantum computer to process quantum images. Finally, obtain the result by the measurement which is the quantum-classical interface.

In 1982, the famous physicist Feynman has recognized more powerful computing ability of quantum computers than that of classical computers [3]. Some of the astonishing properties inherited from quantum computation, such as superposition, significantly reduce both space

Corresponding author's e-mail: olataani@yu.edu.jo

complexity and time complexity. Hence, quantum computers can help us solve the problems that cannot be solved by classical computers efficiently. This is the main reason to develop QImP technologies that are anticipated to grant better capabilities and higher performances than the conventional ones [4], [5].

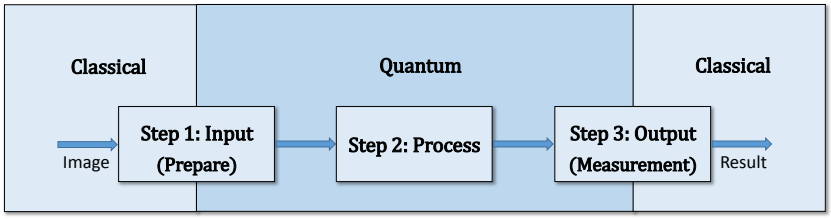

Fig. 1. Framework of QImP

One of the major functions used in many techniques in the discipline of information and image processing is the Fourier Transform Function (FT). It comes as no surprise that its quantum version plays a key role in quantum computational algorithms as it can directly impact the field of image processing. The Quantum Fourier Transform (QFT) is analogous to the classical (FT) with an additional benefit that it can overcome the limitations of classical computations by exploiting the advantages of quantum mechanics [6]. Most known quantum algorithms such as Shor's factoring algorithm [7] and Grover's searching algorithm [8] incorporate QFT as a subroutine. Those algorithms themselves are integrated in a lot of quantum applications like quantum error-correction, encryption and image processing [9]-[11]. While QFT is undoubtedly one of the most important transformations that has a wide range of applications, it is not yet thoroughly investigated.

To understand QImP, it is important to introduce the basics of quantum states and quantum gates [12]. In Quantum Computing, the states of a quantum particle are called qubits (quantum bits). Somewhat analogous to their Boolean counterparts, a quantum particle can exist in two fundamentally distinct states or basis states such as an electron spins of $\pm\frac{1}{2}$ or two orthogonal polarizations of a photon. In the Dirac notation, these states are denoted as $|0\rangle$ and $|1\rangle$. However, unlike Boolean variables a quantum particle can also exist in a superposition of the basis states. The corresponding state space is a 2-dimensional complex Hilbert space $\mathcal{C}^2$, spanned by these two basis states. An arbitrary qubit $|\boldsymbol{\alpha}\rangle$ in a state of superposition can be expressed either using the Dirac notation as a linear combination of the two basis states, or in the equivalent 2×1 vector as, $|\boldsymbol{\alpha}\rangle = a_0|0\rangle + a_1|1\rangle = [a_0 \quad a_1]^T$. Where the quantities a_0 and a_1 represent the amplitudes, the probability of observing the above particle in states $|0\rangle$ and $|1\rangle$ are respectively $|a_0|^2$ and $|a_1|^2$.

Since a_0 and a_1 are complex quantities, they possess both magnitudes as well as phases. A global phase shift can be imparted by multiplying both coefficients with the factor $e^{i\omega}$, where ω is an arbitrary angle. However, such global phase shifts have no observable effect on the qubit. In fact, a global phase can be factored out of $|\boldsymbol{\alpha}\rangle$, so that the amplitude a_0 is strictly real, leading to the following equivalent representation:

$$|\alpha\rangle = \cos\frac{\theta}{2}|0\rangle + e^{i\phi}\sin\frac{\theta}{2}|1\rangle = \begin{bmatrix} \cos\frac{\theta}{2} \\ e^{i\phi}\sin\frac{\theta}{2} \end{bmatrix}$$

A complex quantity $c = a + ib$ can also be represented in a polar form as $me^{i\theta}$, where $m = \sqrt{a^2 + b^2}$ and $\theta = \tan^{-1}\frac{b}{a}$ are its magnitude and phase. This allows us to express any arbitrary qubit in the following manner:

$$|\varphi\rangle = e^{i\omega}\left(\cos\frac{\theta}{2}|0\rangle + e^{i\phi}\sin\frac{\theta}{2}|1\rangle\right)$$

where ω, θ, ϕ are real numbers. The factor $e^{i\omega}$ is referred to as the global phase of the qubit. As the probabilities of observing $|\boldsymbol{\varphi}\rangle$ in the basis states, $P(|0\rangle) = \cos^2\frac{\theta}{2}$, $P(|1\rangle) = \sin^2\frac{\theta}{2}$, do not incorporate the quantity ω. The global state has no observable effect. Although ϕ does not appear either, it does play a significant role when qubits are processed by quantum circuits. Hence, the global phase of the qubit can be dropped without any discernible effect, which can be rewritten as:

$$|\varphi\rangle = \cos\frac{\theta}{2}|0\rangle + e^{i\phi}\sin\frac{\theta}{2}|1\rangle$$

Expressing $|\boldsymbol{\varphi}\rangle$ in the above manner allows us to visualize it as a unit vector in spherical coordinates with $\theta \in [0, \pi]$ being the polar angle, i.e. the angle that the vector $|\boldsymbol{\varphi}\rangle$ forms with the z-axis, while $\phi \in [0, 2\pi]$, the azimuthal angle, i.e. that is between $|\boldsymbol{\varphi}\rangle$ and the xy-plane. In this representation, the unit circle is called the Bloch sphere. Bloch sphere representation is a very handy visualization tool in investigating the role of the quantum equivalents of Boolean gates. The vectors $|0\rangle$ and $|1\rangle$ are directed towards and against the z-axis; and can be regarded as the north and south poles of the Bloch sphere. Similarly, those of the form $\frac{1}{\sqrt{2}}\left(|0\rangle + e^{i\phi}|1\rangle\right)$ lie on the xy-plane and define its equator. The Bloch sphere representation is shown in Fig. 2.

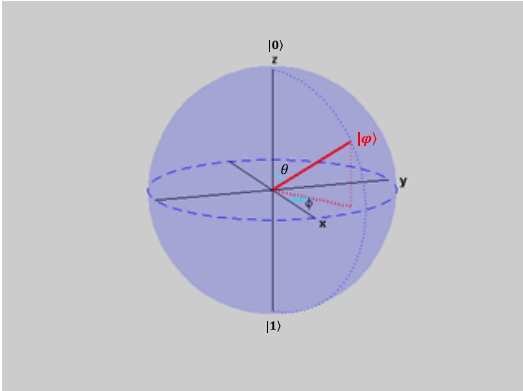

Fig. 2. Block sphere representation of a qubit $|\varphi\rangle = \cos\frac{\theta}{2}|0\rangle + e^{i\phi}\sin\frac{\theta}{2}|1\rangle$. A qubit $|\varphi\rangle$ is shown as a red arrow in this plot

The quantum counterparts of the classical gate are the quantum gate, which simply performs some operations on qubits. One major difference between the two gates is the property of reversibility [13]. A gate is said to be reversible if the input can be uniquely recovered from the output. Hence, there is no loss of information; and as a direct implication, the number of outputs should be equal to the number of inputs.

The quantum gates are reversible and correspond to linear transformations on individual qubits [12]. These transformations can be expressed as matrices. In such matrices, if the gate acts on n input qubits, the matrix will be of size $2^n \times 2^n$. As a direct outcome of

Schrodinger's equation, such matrices must be unitary and have determinants of unity. It is often the case that for the sake of convenience, a quantum gate is represented by a matrix with $\det(\mathbf{U}) \neq 1$. In such cases, its equivalent transformation can be obtained simply by multiplication with an appropriate scalar. Any gate G transforms the input state $|\varphi\rangle$ into the 2^n vector $U_G|\varphi\rangle$ representing the output qubits. Here $U_G|\varphi\rangle$ is the result of premultiplying U_G with$|\varphi\rangle$.

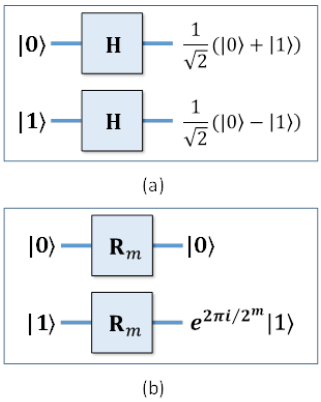

Fig. 3. a) Hadamard gate, b) Phase shift gate

One of the most popular gates that is important to the subject of this paper is the Hadamard gate (**H**). It acts on a single qubit; and creates an equal superposition of the input state. It maps the basis state $|0\rangle$ to $\frac{1}{\sqrt{2}}(|0\rangle + |1\rangle)$ and state $|1\rangle$ to $\frac{1}{\sqrt{2}}(|0\rangle - |1\rangle)$. Another commonly used set of gates is phase-shift gates ($\boldsymbol{R}_m$) which is a family of single-qubit gates. Each integer $m \geq 2$ leaves the basis state $|0\rangle$ unchanged; and shifts the phase of the state $|1\rangle$ of the input by a factor of $e^{2\pi i/2^m}$. The structure of the gates Hadamard and phase-shift gate are shown in Fig. 3. They can be represented by the unitary operators.

$$\mathrm{H} = \frac{1}{\sqrt{2}}\begin{bmatrix}1 & 1\\ 1 & -1\end{bmatrix}, \text{ and } \mathrm{R_m} = \begin{bmatrix}1 & 0\\ 0 & e^{2\pi i/2^m}\end{bmatrix}$$

The rest of this paper is organized as follows. In section II, we present the most relevant work in literature review. In sections III, we introduce the basic framework of QImP based on the quantum probability image encoding (QPIE) model for quantum image representation (QImR). In section III, we show the experimental demonstration for the quantum Fourier transform with its implementation on sample images. Finally, in section IV, we conclude the work presented in this paper; and give perspectives for future work.

II. LITERATURE REVIEW

Utilizing quantum power in the field of image processing can be traced back to the late nineties [14]. It was followed by many attempts that fall under one of two categories [5], [15]. The first is a Quantum-assisted that aims to exploit the properties of quantum computing to improve classical image processing tasks and applications. The second is referred to as a classically inspired in that it focuses on extending classical image processing tasks and applications to the quantum computing framework. This follows the expectation that quantum computing hardware will soon be physically realized [5]. Therfore, several QImP models have been proposed.

In 2003, Venegas-Andraca and Bose proposed a technique for storing, processing and retrieving images based on quantum techniques. The proposed technique uses the "qubit

lattice" model for images representation as quantum images [16]. Since each pixel is represented using a single qubit, it requires a 2^n qubits to represent an image of 2^n pixels. The proposed model is only a quantum-analog presentation of classical images without any benefit from quantum efficiency and speed-up efficiency. In a more recent study, a flexible representation of quantum images (FRQI) was proposed by Le, P.Q. etc al. [17]. Their representation can be used for polynomial image preparation, image compression, and image processing techniques. The technique is basically based on integrating the pixel value and position information in an image into a $(n+1)$ qubit quantum states as follows, $\frac{1}{\sqrt{2^n}}\sum_{k=0}^{2^n-1}(\cos\theta_k\,|0\rangle + \sin\theta_k|1\rangle)\;|k\rangle$, where the angle θ_k in a single qubit encodes the pixel value of the corresponding position $|k\rangle$.

The results of simulations for different experiments, including images storage, retrieval and line detection in binary images, are done by applying the quantum Fourier transform as the processing operation. The proposed FRQI provides a foundation to express images and explore theoretical and practical fields of image processing in quantum computing.

As an extension from a 2D grayscale representation, Sun et al. provide the multichannel representation for quantum images (MCQI) as a new model for colored images (RGB) representation [18]. The model uses the three channels of a colored image (R, G, and B channels) to represent different color information of the image while using the state normalization technique. Since there are three channels, the model is accomplished by assigning three qubits to encode color where the RGB information of an image is stored simultaneously. The proposed model is represented by the equation as follows, $\frac{1}{2^{n+1}}(\sum_{i=0}^{2^{2n}-1}|C^i_{RGB\alpha}\rangle \otimes |i\rangle$, where the color information $|C^i_{RGB\alpha}\rangle$_ encoding the RGB channels information is defined as:

$$\begin{aligned}\left|\mathrm{C}^{\mathrm{i}}_{\mathrm{RGB}\alpha}\right\rangle = \cos\theta^{\mathrm{i}}_{\mathrm{R}}\left|000\right\rangle + \cos\theta^{\mathrm{i}}_{\mathrm{G}}\left|001\right\rangle + \cos\theta^{\mathrm{i}}_{\mathrm{B}}\left|010\right\rangle + \cos\theta^{\mathrm{i}}_{\alpha}|011\rangle + \; +\sin\theta^{\mathrm{i}}_{\alpha}|100\rangle \\ + \sin\theta^{\mathrm{i}}_{\mathrm{G}}\left|101\right\rangle + \sin\theta^{\mathrm{i}}_{\mathrm{B}}\left|110\right\rangle + \sin\theta^{\mathrm{i}}_{\alpha}|111\rangle\end{aligned}$$

where $\{\theta^i_R, \theta^i_G, \theta^i_B\} \in [0, \pi/2]$ are three angles encoding the colors of the R, G, and B channels of the i^{th} pixel, respectively; and θ_α is set to 0 to make the two coefficients constant ($\cos\theta_\alpha = 1$ and $\sin\theta_\alpha = 0$) to carry no information.

A novel enhanced quantum representation (NEQR) was presented by Yi Zhang *et. al.* [19]. The proposed representation improves the latest flexible representation of quantum images (FRQI) by Le, P.Q. et al. [17]. The novel method uses the basis state $|f(k)\rangle$ of d qubits to store the pixel value instead of angle information encoded in a qubit as in FRQI. That is, an image is encoded as a quantum state $\frac{1}{\sqrt{2^n}}\sum_{k=0}^{2^n-1}|f(k)\rangle\;|k\rangle$, where$|f(k)\rangle = |\mathrm{C}^0_\mathrm{k}\mathrm{C}^1_\mathrm{k}\ldots\mathrm{C}^{\mathrm{d}-1}_\mathrm{k}\rangle$.

Yao *et. al.* proposed a new quantum probability image encoding (QPIE) model for quantum image representation [20]. The model encodes the image pixel values in probability amplitudes and their positions into computational basis states. The model speeds up the computation time required for either image representation or QImP techniques, which represent the main potential of QImP fields for highly efficient image processing in the big data era. Table 1 provides a detailed comparison between some methods mentioned in the literature.

TABLE 1
A COMPARISON BETWEEN DIFFERENT QUANTUM IMAGE REPRESENTATION MODELS
(FRQI, MCQI, NEQR, AND QPIE)

Image Representation	**FRQI**	**MCQI**	**NEQR**	**QPIE**
Quantum State	$\frac{1}{2^m}(\sum_{k=0}^{2^{2m-1}}(\cos\theta_k\|0\rangle + \sin\theta_k\|1\rangle)\|k\rangle$	$\frac{1}{2^{n+1}}(\sum_{i=0}^{2^{2n}-1}\|C^i_{RGB\alpha}\rangle \otimes \|i\rangle$	$\frac{1}{2^m}(\sum_{d=0}^{2^{2m-1}}\|f(k)\rangle\|k\rangle$	$\|f(k)\rangle = \sum_{k=0}^{2^{2m-1}} c_k\|k\rangle$
Pixel-Value Qubit	1	C	d	0
Pixel Value	θ_k	$\|C^i_{RGB\alpha}\rangle = cos\theta^i_R\|000\rangle + cos\theta^i_G\|001\rangle + cos\theta^i_B\|010\rangle + cos\theta^i_\alpha\|011\rangle + +sin\theta^i_\alpha\|100\rangle + sin\theta^i_G\|101\rangle + sin\theta^i_B\|110\rangle + sin\theta^i_\alpha\|111\rangle$	$f(k) = C^0_k C^1_k \dots C^{d-1}_k$	c_k
Pixel-Value Encoding	Angle	Probability Amplitude	Basis of Qubits	Probability Amplitude

Only few works in literature addressed the general applications of QFT for image processing; and to the best of our knowledge all were used in either watermarking or enhancing security. A recent study in [21] has utilized Quantum Fourier Transformation (QFT) in a protocol to enhance the security of NEQR of quantum images with a blind trent. The suggested protocol uses a QFT and key encrypted signature for image security. A reordered output Qubit of QFT with permutation of a blind trent is used to improve the security of the protocol. This protocol was shown to enhance the transfer of images with a secured and efficient secret key. Another algorithm that is based on QFT for image encryption is introduced in [22]. The encryption algorithm proposed is supported by quantum Fourier transformation. As in [21], the algorithm showed an enhanced image security.

In [23], a Quantum Image classification schema which uses quantum K-Nearest-Neighbor algorithm is introduced. To achieve parallel computing of similarity, features extracted from classical computers are inputted into a quantum superposition state. The image is then classified by quantum measurement after using a minimum quantum search algorithm. Results showed high classification accuracy while improving classification efficiency.

III. FRAMEWORK OF QUANTUM IMAGE PROCESSING

Earlier in this paper, we discussed the basics of quantum computations that are important to the scope of this paper. However, before introducing our experimental framework, it is important to first discuss the quantum Fourier Transform (QFT) itself.

A) Quantum Fourier Transform

The quantum Fourier transform acts on a quantum state $|\mathbf{x}\rangle = [x_0 \quad x_1 \quad \cdots \quad x_{N-1}]^T$. It maps it to a quantum state $|\mathbf{y}\rangle = [y_0 \quad y_1 \quad \cdots \quad y_{N-1}]^T$ according to the formula:

$$y_k = \frac{1}{\sqrt{N}}\sum_{j=0}^{N-1} x_j w_n^{jk}, \qquad k = 0, 1, \dots, N-1,$$

where $w_n = e^{\frac{-2\pi i}{N}}$ is a primitive N^{th} root of unity.

The factor w, which is called the primitive roots of unity, can be viewed as a phase introduced by the QFT. Equivalently, the QFT can be viewed as a unitary matrix or a quantum gate acting on quantum state vectors. The unitary matrix QFT_N is given by:

$$QFT_N = \frac{1}{\sqrt{N}} \begin{bmatrix} 1 & 1 & 1 & 1 & \dots & 1 \\ 1 & w_n & w_n^2 & w_n^3 & \cdots & w_n^{N-1} \\ 1 & w_n^2 & w_n^4 & w_n^6 & \cdots & w_n^{2(N-1)} \\ 1 & w_n^3 & w_n^6 & w_n^9 & \cdots & w_n^{3(N-1)} \\ \vdots & \vdots & \vdots & \vdots & & \vdots \\ 1 & w_n^{N-1} & w_n^{2(N-1)} & w_n^{3(N-1)} & \cdots & w_n^{(N-1)(N-1)} \end{bmatrix},$$

where w_n is defined as above.

Therefore, the n −qubit QFT transforms an input state $|\mathbf{x}\rangle$ to an output state $|\mathbf{y}\rangle$ as follows: $|\mathbf{y}\rangle = QFT_N|\mathbf{x}\rangle$.

This linear transformation is unitary; and can be realized using a quantum circuit that consists of a set of quantum gates connected together (Fig. 4). The gates labelled **H** are Hadamard gates as described before; and the gates labelled $\mathbf{R}_m$ represent a series of one-qubit phase shift gates. However, in the QFT circuit, each $\mathbf{R}_m$ gate is controlled by another qubit. This means that depending on the value of the control bit, controlled$-\mathbf{R}_m$ gate performs the identity transformation, or the $\mathbf{R}_m$ (i.e. phase shift) transformation. The controlled$-\mathbf{R}_m$ is indicated by a large dot connected to the gate by a vertical line; and the unitary matrix is given by:

$$R_m = \begin{bmatrix} 1 & 0 & 0 & 0 \\ 0 & 1 & 0 & 0 \\ 0 & 0 & 1 & 0 \\ 0 & 0 & 0 & e^{2\pi i/2^m} \end{bmatrix}$$

This circuit is implemented by the sequence of the shown operations, where the bit values of the result appear in reversed order. The qubits must be reversed; and this can be achieved by a sequence of SWAP operations on pairs of qubits (not shown in the circuit).

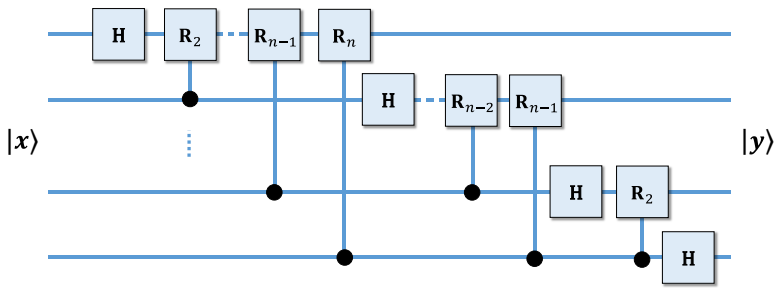

Fig. 4. A schematic of the quantum circuit which implements the n-qubit QFT using qubit-selective Hadamard and two- qubit controlled-phase gates

B) A Framework for Quantum Image Representation

Of particular interest in our context is the recent work of Yao *et. al.* [20] where a QImR model is introduced. It is based on encoding the image transformation in a pure quantum state which provides a flexible representation of quantum images.

Given a 2D image $F = (F_{i,j})_{M\times L}$, $F_{i,j}$ represents the pixel value at position (i, j) with $i = 1, \dots, M$ and $j = 1, \dots, L$. The quantum representation model adopted in this paper is to convert the $(M \times L)$ matrix F into a column vector f of length ML. The procedure is made by letting the first M elements of f be the first column of F, the next M elements, the second column, etc. such that:

$$f = \begin{bmatrix} F_{1,1} & F_{2,1} & .... & F_{M,1} & F_{1,2} & .... & F_{i,\,j} & .... & F_{M,L} \end{bmatrix}^{T}$$

The vector f can be mapped into a pure quantum state of n qubits, that is

$$|\mathrm{f}\rangle = \sum_{\mathrm{k}=0}^{2^{\mathrm{n}}-1} \mathrm{c_k}\,|\mathrm{k}\rangle,$$

where $|k\rangle$ represents the (i, j) position for each pixel with $n = \lceil log_2(ML) \rceil$; and c_k represents the pixel value such that,

$$\mathrm{c_k} = \begin{cases} \dfrac{\mathrm{F_{i,j}}}{\sqrt{\sum_{\mathrm{k}=0}^{2^{\mathrm{n}}-1} \mathrm{F_{i,j}}^2}}, & \mathrm{k} < \mathrm{ML} \\ 0 & \mathrm{k} \geq \mathrm{ML} \end{cases}$$

This step is important to ensure that the final quantum state of pixel values is normalized. By adopting this procedure, the final quantum images are represented in the form of a normalized state which captures information about colors and their corresponding positions in the images.

In our work, we consider the special case where $ML = N = 2^n$. Image transformation is linear in nature. In the quantum context, the linear transformation can be represented as follows: given an input image state $|f\rangle$, the output image state $|g\rangle = \mathbf{U}|f\rangle$. The corresponding unitary operator **U** is given by:

$$U = \mathrm{QFT}_N = \frac{1}{\sqrt{N}} \begin{bmatrix} 1 & 1 & 1 & 1 & \dots & 1 \\ 1 & w_n & w_n^{2} & w_n^{3} & \cdots & w_n^{N-1} \\ 1 & w_n^{2} & w_n^{4} & w_n^{6} & \cdots & w_n^{2(N-1)} \\ 1 & w_n^{3} & w_n^{6} & w_n^{9} & \cdots & w_n^{3(N-1)} \\ \vdots & \vdots & \vdots & \vdots & & \vdots \\ 1 & w_n^{N-1} & w_n^{2(N-1)} & w_n^{3(N-1)} & \cdots & w_n^{(N-1)(N-1)} \end{bmatrix}$$

where $w_n = e^{\frac{-2\pi i}{2^n}}$

In general, a comparison of image processing performed by the classical and quantum methods is illustrated in Fig. 5. Classically, the image is represented as a matrix; and it is encoded with 2^n bits. The image transformation is conducted by matrix computation. In contrast, the same image is represented as a quantum state; and encoded in n qubits. The quantum image transformation is performed by unitary operator **U**.

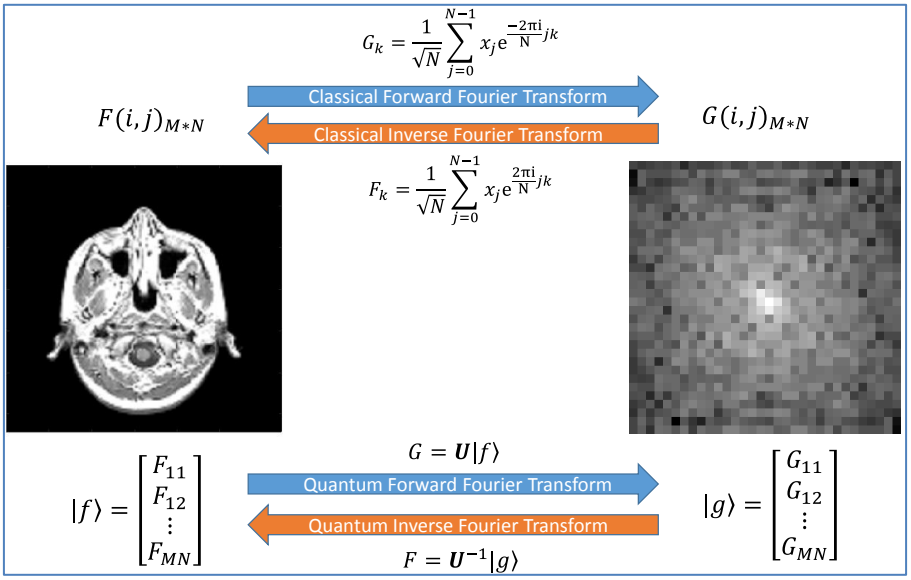

Fig. 5. Comparison of image encoding, processing, and decoding by classical and quantum methods

IV. EXPERIMENTAL DEMONSTRATION

For demonstrating our framework, a classical computer is used to simulate the experiments on quantum images. The simulations are based on linear algebra with complex vectors as quantum states and unitary matrices as unitary transforms. MATLAB 2015a is used as a programming language; and the experiments are performed on desktop computer with Intel Core 2 Duo 1.86 GHz CPU and 2 GB RAM.

A set of different sample images is used to experimentally demonstrate the quantum image transforms while comparing them with the conventional transforms. As a simple test image, a window of a 2×2 pixels cropped from an image is chosen. The image encoding and processing require four qubits represented by a 4×1 column vector. The image transformation operator that need to be considered is defined by $\mathbf{U} = QFT_4$. That is

$$QFT_4 = \frac{1}{2} \begin{bmatrix} 1 & 1 & 1 & 1 \\ 1 & i & -1 & -i \\ 1 & -1 & 1 & -1 \\ 1 & -i & -1 & i \end{bmatrix}$$

The corresponding quantum circuit with the actual gate sequences in our sample experiment is shown in Fig. 6. If we split the circuit up, each unitary transformation output is implemented separately as illustrated in the figure.

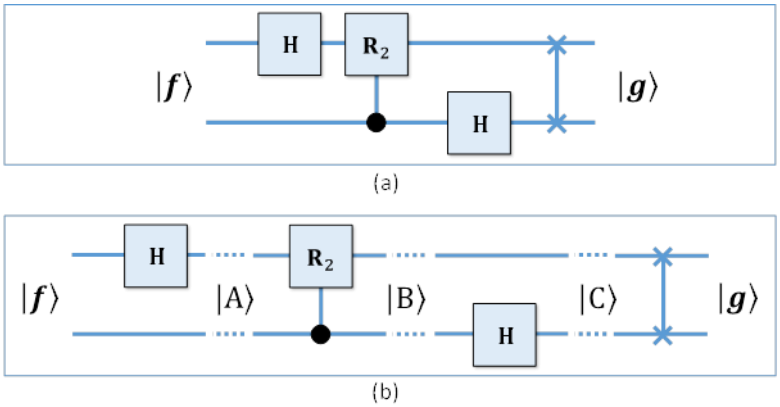

Fig. 6. a) Quantum circuit that implements a 2-qubit QFT, b) The serial implementation of the QFT circuit

The output QFT can be obtained by evaluating the decomposed circuit in Fig. 4b with $|\mathrm{A}\rangle = \boldsymbol{U_1}|f\rangle$, $|\mathrm{B}\rangle = \boldsymbol{U_2}|\mathrm{A}\rangle$, $|\mathrm{C}\rangle = \boldsymbol{U_3}|\mathrm{B}\rangle$, $|g\rangle = \boldsymbol{U_4}|\mathrm{C}\rangle$.

It can be easily shown that,

$$\boldsymbol{U}_1 = \frac{1}{\sqrt{2}}\begin{bmatrix} 1 & 0 & 1 & 0 \\ 0 & 1 & 0 & 1 \\ 1 & 0 & -1 & 0 \\ 0 & 1 & 0 & -1 \end{bmatrix}, \boldsymbol{U}_2 = \frac{1}{\sqrt{2}}\begin{bmatrix} 1 & 0 & 0 & 0 \\ 0 & 1 & 0 & 0 \\ 0 & 0 & 1 & 0 \\ 0 & 0 & 0 & i \end{bmatrix}, \boldsymbol{U}_3 = \begin{bmatrix} 1 & 1 & 0 & 0 \\ 1 & -1 & 0 & 0 \\ 0 & 0 & 1 & 1 \\ 0 & 0 & 1 & -1 \end{bmatrix},$$

$$\boldsymbol{U}_4 = \begin{bmatrix} 1 & 0 & 0 & 0 \\ 0 & 0 & 1 & 0 \\ 0 & 1 & 0 & 0 \\ 0 & 0 & 0 & 1 \end{bmatrix}.$$

Then we have, $\boldsymbol{U} = \boldsymbol{U_4 U_3 U_2 U_1} = \frac{1}{2}\begin{bmatrix} 1 & 1 & 1 & 1 \\ 1 & i & -1 & -i \\ 1 & -1 & 1 & -1 \\ 1 & -i & -1 & i \end{bmatrix}$.

This is the same as what can be obtained by doing the calculations directly (QFT_4). Therefore, we have verified that this circuit does indeed perform the QFT.

The QImP method discussed earlier is applied to different selected images. Fig. 7 shows sample images that were chosen along with their Fourier transformations using the classical FFT and QFT. The reconstructed images conducted by the inverse FFT and QFT are also plotted. It is visually clear that the original and the reconstructed quantum images are identical (image 5 for example). This result can also be inferred by calculating the Mean-squared error (MSE). Specifically, the resulting transformation of image 5 has a MSE of value 0 (last column in table 2) defined by the equation,

$$\mathrm{MSE} = \frac{1}{\mathrm{M} * \mathrm{N}} \sum_{\mathrm{m}=1}^{\mathrm{M}} \sum_{\mathrm{n}=1}^{\mathrm{N}} [\mathrm{F}'(\mathrm{m},\mathrm{n}) - \mathrm{F}(\mathrm{m},\mathrm{n})]^2,$$

where M and N are the number of rows and columns in the compared images (the original image $\mathrm{F}(x, y)$ and the reconstructed image $\mathrm{F}'(x, y)$), respectively.

Mean-Squared Error (MSE) assesses the quality of an image. Values of MSE may be used for comparative purposes. Two or more images may be compared using their MSEs as a measurement of image distortion because they can represent the overall gray-value error contained in the entire image, and are mathematically tractable as well [21]. MSE values are always non-negative; and values closer to zero are better. In our simulations, most MSE results are of zero value or very close to zero as represented in Table 2.

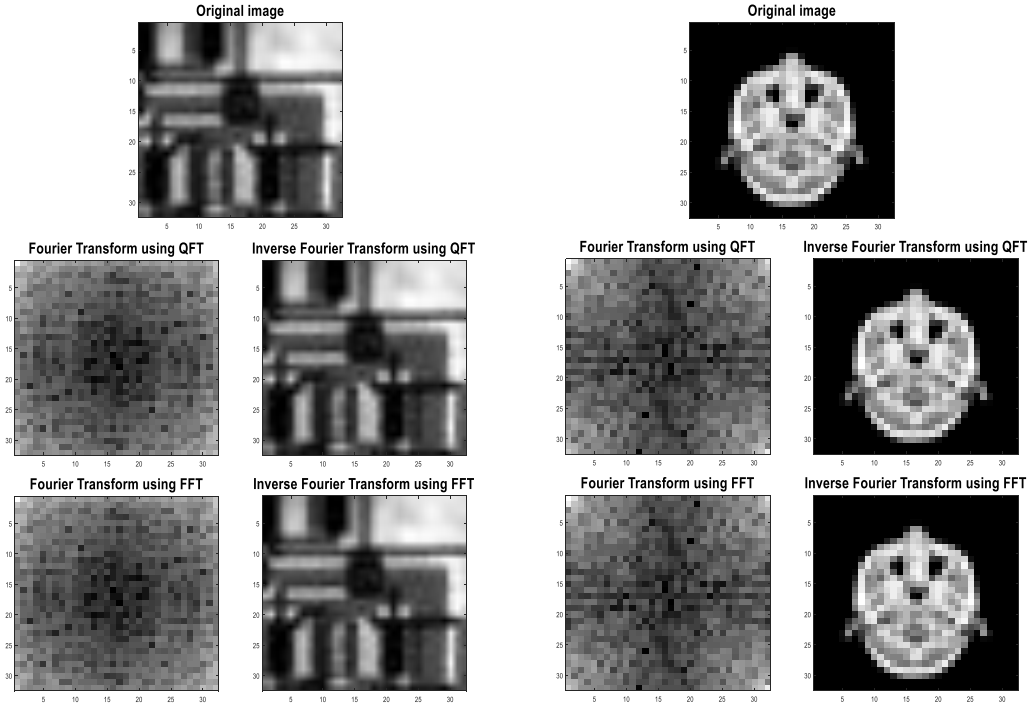

Fig. 7. Sample images used in the simulation (image 1 to the left, image 5 to the right)

Other quality measurements between the original and reconstructed images such as Peak Signal-to-Noise Ratio (PSNR) and Structural Similarity Index (SSIM) [25], [26] are considered. The PSNR represents a measure of the peak error. The lower the value of MSE, the lower the error is. A higher PSNR generally indicates that the reconstruction is of higher quality. Based on PSNR results in our simulation, QFT is shown to perform better compared to FFT (Table 2). It is evaluated using the following equation:

$$\mathrm{PSNR} = 10 * \mathrm{Log}_{10}\left(\frac{\mathrm{peakval}^{\,2}}{\mathrm{MSE}}\right),$$

where peakval is taken from the range of the image datatype (e.g. for unit 8 image it is 255). The Structural Similarity Index (SSIM) is used for measuring the similarity between two images: the original image $F(x, y)$ and the reconstructed image $F'(x, y)$. In general, a higher SSIM value indicates higher image quality. Our simulations give similar results for both QFT and FFT (Table 2). It is calculated using the following equation:

$$\mathrm{SSIM} = \frac{(2\mu_{F'}\mu_F + c_1)(2\sigma_{F'F} + c_2)}{(\mu_{F'}^2 + \mu_F^2 + c_1)(\sigma_{F'}^2 + \sigma_F^2 + c_2)}$$

where:

$\mu_{F'}$ and μ_F are the mean of $F'(x,y)$ and $F(x,y)$ respectively.

$\sigma_{F'}$ and σ_F are the variance of $F'(x,y)$ and $F(x,y)$ respectively.

$c1 = (K_1 L)^2$and $c2 = (K_2 L)^2$ are variables to stabilize the division with weak denominator

$L = 2^{\#\ of\ Bits\ per\ pixel} - 1$

$k_1 = 0.01$ and $k_2 = 0.03$ by default.

Table 2 provides a sample comparison between the two methods (FFT and QFT) with respect to (Forward and inverse elapsed time, MSE, PSNR, and SSIM) applied to five different images. Figs. 8 and 9 show the results for the set of test images with respect to MSE and SSIM respectively. The results indicate that both methods FFT and QFT perform similarly on a classical computer. We should emphasize here that it is expected that the QFT method outperforms the classical one if experiments were conducted on a quantum computer.

One of the main goals in quantum computing is to design quantum algorithms that are more efficient (i.e. faster) than their classical counterparts. This goal usually has an implicit assumption that both quantum and classical algorithms are to be executed on general-purpose computers. Unfortunately, the quest for QImP algorithms running on general-purpose computers has left behind the superiority of quantum image processing algorithms especially with respect to time complexity.

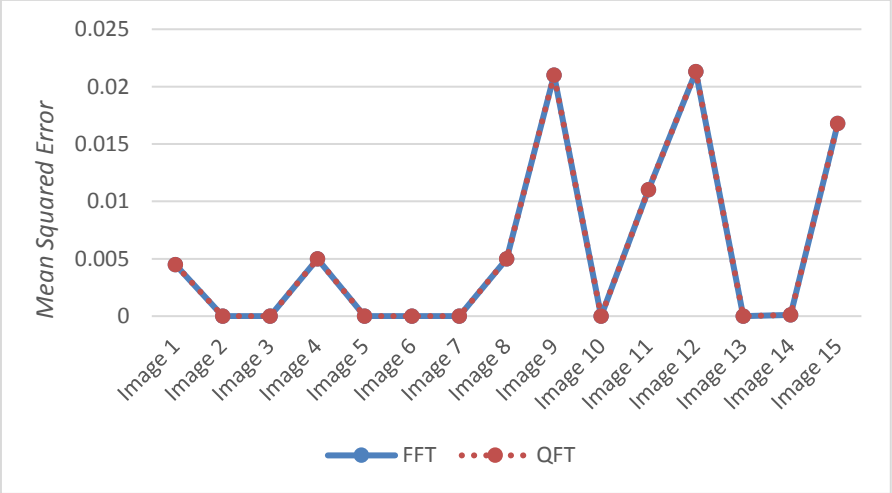

Fig. 8. The MSE results of the two methods (FFT and QFT) for different test images

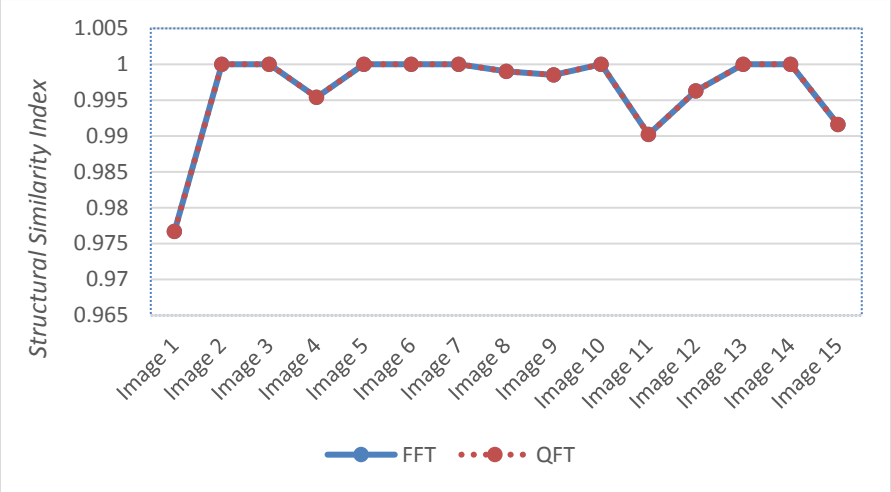

Fig. 9. The SSIM results of the two methods (FFT and QFT) for different test images

Moreover, the relationship between the consumption time needed to reconstruct the quantum image with respect to the resolution of the image is also considered in our simulations (illustrated in Fig. 10). The QImP method performs better than the classical one specifically with when the number of qubits is less than 5 (i.e. $n < 5$).

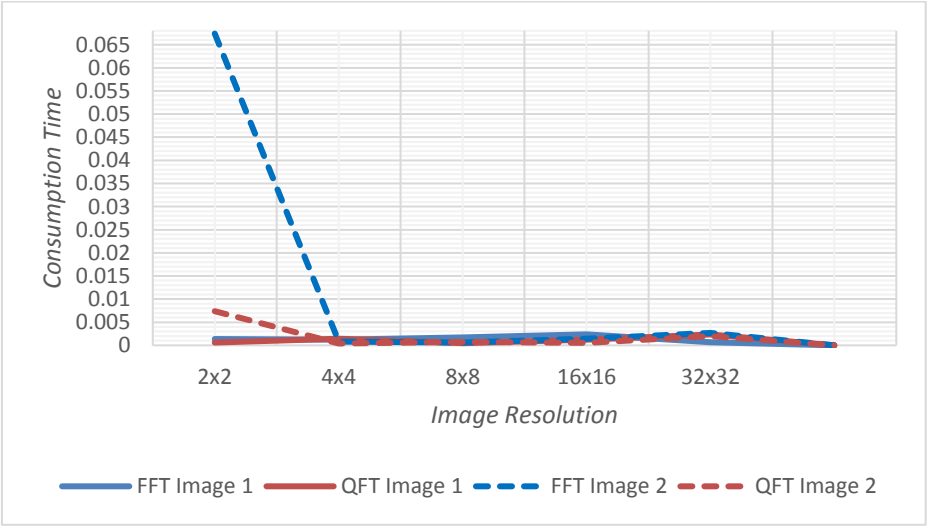

Fig. 10. Consumption time for different image resolutions

TABLE 2
A COMPARISON BETWEEN THE TWO METHODS (FFT AND QFT) FOR FIVE DIFFERENT IMAGES

Image No.	Method	Forward Elapsed Time	Reconstruction Elapsed Time	Mean-squared error (MSE)	Peak Signal-to-Noise Ratio (PSNR)	Structural Similarity Index (SSIM)
1	*FFT*	0.002033	0.000804	0.0045	46.8906	0.9767
	QFT	0.002367	0.002242	0.0045	46.8906	0.9767
2	*FFT*	0.000448	0.00063	0	319.4987	1
	QFT	0.002154	0.001708	0	229.4296	1
3	*FFT*	0.000509	0.000522	0	315.9064	1
	QFT	0.002061	0.002361	0	230.783	1
4	*FFT*	0.000819	0.000476	0.005	45.9777	0.9954
	QFT	0.002159	0.00165	0.005	45.9777	0.9954
5	*FFT*	0.000553	0.000598	0	319.7095	1
	QFT	0.001844	0.001882	0	230.2293	1

V. CONCLUSION AND FUTURE WORK

In conclusion, the potential of quantum computing in the field of image processing is demonstrated. A QImP model is used where image information is encoded in a pure quantum state where pixel values of an image of interest are encoded in the probability amplitudes while the pixel positions are encoded in the computational basis states. Moreover, the implementation of the model on sample images is illustrated. Their encoding, processing, and decoding are experimentally demonstrated. The processing operations are performed classically using FFT and in a quantum context using QFT. These resulting transforms are compared; and the comparison results are reported. In this comparison, different measures of image quality are used for both FFT or QFT reconstructed images. Results from a three quality measures are reported: The Mean-Squared Error (MSE) to estimate the error between two images, the Peak Signal-to-Noise Ratio (PSNR) to evaluate the quality of reconstructed image and the Structural Similarity Index (SSIM) to assess the similarity between two images. In general, the QFT results are shown to be similar to FFT in all cases.

Our experiment serves as the first experimental study towards practical applications of quantum computers for image processing. However, it might be of interest not to read the output image itself only but to find some significant statistical characteristics or useful global features about image data. It is a possibility to explore this area instead of decoding the image explicitly. In addition to the theoretical base presented in this paper, quantum computing still has much to offer. The QFT model can be employed in other areas such as machine learning, face and pattern recognition, and image and video coding.

REFERENCES

[1] P. Ioannis, *Digital Image Processing Algorithms and Applications*, John Wiley & Sons, 2000.

[2] D. Pham, C. Xu, and J. Prince, "Current methods in medical image segmentation," *Annual Review of Biomedical Engineering*, vol. 2, no. 2000, pp. 315-337, 2000.

[3] R. Feynman, "Simulating physics with computers," International Journal of Theoretical Physics, vol. 21, no. 6/7, pp.467-488, 1982.

[4] A. Iliyasu, "Towards realising secure and efficient image and video processing applications on quantum computers," *Entropy*, vol. 15, no. 8, pp. 2874-2974, 2013.

[5] F. Yan, A. Iliyasu, and P. Le, "Quantum image processing: a review of advances in its security technologies," *International Journal of Quantum Information*, vol. 15, no. 03, pp. 1-18, 2017.

[6] S. Lloyd, M. Mohseni, and P. Rebentrost, "Quantum principal component analysis," *Nature Physics*, vol. 10, no. 9, pp. 631-633, 2014.

[7] W. Shor, "Algorithms for quantum computation: discrete logarithms and factoring," *Proceedings of 35th Annual Symposium on Foundations of Computer Science*, pp. 124-134, 1994.

[8] L. Grover, "Quantum mechanics helps in searching for a needle in a haystack," *Physical Review Letters*, vol. 79, no. 2, pp. 1-4, 1997.

[9] C. Bennett, D. Divincenzo, J. Smolin, and W. Wootters, "Mixed-state entanglement and quantum error correction," *Physical Review A*, vol. 54, no. 5, pp. 3824-3851, 1996.

[10] P. Townsend, "System and method for key distribution using quantum cryptography," *U.S. PatentUS5675648*, issued October 7, 1997.

[11] A. Iliyasu, P. Le, F. Yan, B. Sun, F. Dong, A. Al-Asmari, and K. Hirota, "Insights into the viability of using available photonic quantum technologies for efficient image and video processing applications," *International Journal of Unconventional Computing*, vol 9, pp. 125-151, 2013.

[12] M. Nielsen, I. Chuang, *Quantum Computation and Quantum Information*, Cambridge University Press, UK, 2000.

[13] A. Peres, "Reversible logic and quantum computers," *Physical Review A*, vol. 32, no 6, pp. 3266- 3276, 1996.

[14] A. Vlasov, "Quantum computations and images recognition," *arXiv:quant-ph/9703010*, 1997.

[15] F. Yan, A. Iliyasu, and S. Venegas-Andraca, "A survey of quantum image representations," *Quantum Information Processing*, vol. 15, no. 1, pp. 1-35, 2016.

[16] S. Venegas-Andraca and S. Bose, "Storing, processing, and retrieving an image using quantum mechanics," *Proceedings of Quantum Information and Computation, International Society for Optics and Photonics*, vol. 5105, pp. 137-148, 2003.

[17] P. Le, F. Dong, and K. Hirota, "A flexible representation of quantum images for polynomial preparation, image compression, and processing operations," *Quantum Information Processing*, vol. 10, no. 1, pp. 63-84, 2011.

[18] B. Sun, A. Iliyasu, F. Yan, F. Dong, K. Hirota, "An RGB multi-channel representation for images on quantum computers," *Journal of Advanced Computational Intelligence and Intelligent Informatics*, vol. 17, no. 3, pp. 404-417, 2013.

[19] Y. Zhang, K. Lu, Y. Gao, and M. Wang, "NEQR: a novel enhanced quantum representation of digital images," *Quantum Information Processing*, vol. 12, no. 8, pp. 2833-2860, 2013.

[20] X. Yao, H. Wang, Z. Liao, M. Chen, J. Pan, J. Li, K. Zhang, X. Lin, Z. Wang, Z. Luo, W. Zheng, J. Li, M. Zhao, X. Peng, and D. Suter, "Quantum image processing and its application to edge detection: theory and experiment," *Physical Review X*, vol. 7, no. 3, pp. 1-14, 2017.

[21] E. Sahin and I. Yılmaz, "Security of NEQR quantum image by using quantum fourier transform with blind trent," International Journal of Information Security Science, vol. 7, no. 1, pp. 20-25, 2018.

[22] Y. Liu, B. Zhou, Z. Li, J. Deng, and Z. Cai, "An image encryption method based on quantum fourier transformation," International Journal of Intelligence Science, vol. 8, no. 3, pp. 75-87, 2018.

[23] Y. Dang, N. Jiang, H. Hu, Z. Ji, and W. Zhang, "Image classification based on quantum k-nearest-neighbor algorithm," Quantum Information Processing, vol. 17, pp. 1-18, 2018.

[24] Z. Wang and A. Bovik, "Mean squared error: love it or leave it? a new look at signal fidelity measures," *IEEE Signal Processing Magazine*, vol. 26, no. 1, pp. 98-117, 2009.

[25] Z. Wang and A. Bovik, "A universal image quality index," *IEEE Signal Processing Letters*, vol. 9, no. 3, pp. 81-84, 2002.

[26] Z. Wang, A. Bovik, H. Sheikh, and E. Simoncelli, "Image quality assessment: from error visibility to structural similarity," *IEEE Transactions on Image Processing*, vol. 13, no. 4, pp. 600-612, 2004.